Research Square

Preprints are preliminary reports that have not undergone peer review.
They should not be considered conclusive, used to inform clinical practice,
or referenced by the media as validated information.

High performance Juncus effusus cellulosic adsorbent modified with citric acid and magnetic Fe3O4 for dye wastewater

Keming Zhou
East China University of Science and Technology
Lianpeng Yan
East China University of Science and Technology
Rui Zhang (r.zhang@ecust.edu.cn)
East China University of Science and Technology
Xuedong Zhu
East China University of Science and Technology

Research Article

Keywords: Cellulose-based, Juncus effusus, Magnetic adsorbent, Dye adsorption

Posted Date: September 13th, 2022

DOI: https://doi.org/10.21203/rs.3.rs-2036902/v1

License: This work is licensed under a Creative Commons Attribution 4.0 International License.
Read Full License

Abstract

Eco-friendly cellulose-based magnetic adsorbents have attracted great attention in the field of dye adsorption recently. Herein, we utilized the pith of biomass Juncus effusus (JE) to synthesize a novel type of magnetic adsorbents for the treatment of wastewater containing methylene blue (MB). After employing citric acid (CA) for esterified modification and then loading Fe3O4 upon JE, the obtained magnetic citric acid-modified JE pith powders (M-CA/JEPP) showed outstanding adsorption properties. For 50 mg/L MB dye solution, the adsorption efficiency could reach 98.34% within 10 min under basic condition and the maximum adsorption capacity was 293.132 mg/g at 303 K. Moreover, magnetization overcomes the disadvantages of JE powders density being small which is very difficult to collect. In the other words, this magnetic adsorbent has excellent reusability and it is easily to be separated from water, which provides new insights for development of cellulose-based adsorbents to remove dye in aqueous systems.

Introduction

Water shortage and pollution have threatened people's daily life all over the world. Therefore, improving the removal efficiency of water contaminants to make full use of water resources is of great practical significance to realize sustainable development. (Chen et al. 2020; Shannon et al. 2008) Organic dyes are widely used for dyeing in textile, papermaking, plastics, leather, food, cosmetics and other fields, which is one of the most concerned pollutants in the water. During dyeing process, 10–15% of the dyestuffs are discharged directly into the wastewater. (Yeamin et al. 2021) These organic dyes which are toxic, degradable and have stable structure pour into the hydrosphere with wastewater, causing great harm to the environment and human. (Chen et al. 2021; Li et al. 2020) In particular, methylene blue (MB) is a characteristic cationic dye that has been extensively used in various industries due to its outstanding water solubility and color stability. However, it not only endangers aquatic organisms, but also bring people health problems such as dermatitis, jaundice, nausea, vomiting, and allergies. (Jawad et al. 2020)

A variety of physical, chemical, and biological technology have been taken to treat dye wastewater, (Crini and Lichtfouse 2018) such as flocculation, (Verma et al. 2012) oxidation, (Paździor et al. 2019) adsorption, (Zhao et al. 2021) ion exchange, (Cseri et al. 2021) membrane filtration, (Zeng et al. 2021) electrochemistry, (Brillas and Martínez-Huitle 2015) biodegradation and phytoremediation, (Bhatia et al. 2017) etc. Among these technologies, adsorption has attracted more attention because it is efficient, simple and relatively low cost. (Ahsan et al. 2020) Traditional adsorbents include activated carbon, (Wang et al. 2021; Wong et al. 2018) zeolite, (Aljerf 2018; Alver and Metin 2012) carbon nanotubes, (Aliabadi and Mahmoodi 2018; Zhang et al. 2020) etc., most of them are limited in application due to their high operating costs and hard regeneration. (Alsbaiee et al. 2016; Jiang et al. 2018) So renewable, low-cost and non-toxic biomass-based cellulosic adsorbents are becoming increasingly popular and have broad prospects in the field of dye wastewater treatment. (Shao et al. 2021; Varghese et al. 2018)

Some parts of many plants are inexpensive adsorbents inherently, but they always have low adsorption capacity. (Değermenci et al. 2019; Han et al. 2011; Tanyildizi 2011) Thus, chemical modification is often used to increase the adsorption capacity of these cellulosic adsorbents, and esterification modification is one of them. It is a common modification method to introduce carboxyl functional groups by make cellulose esterification with organic acids such as citric acid. (Gong et al. 2006; Gong et al. 2008; Sun et al. 2015) Zhao and Zhou (Zhao and Zhou 2016) used citric acid to modify extraction residue of Salvia mitiorrziza Bge which exhibited a better dye removal capacity. In addition, Peng (Peng et al. 2021) et al. prepared malic acid-modified corn stalk pith to achieve effective adsorption performance on dyes and oils. Although the adsorption capacity of these adsorbents has been improved, it is difficult to separate them from treated wastewater.

Juncus effusus (JE) is a kind of cheap and accessible cellulose-based biomass whose pith have a 3D network structure naturally. (Liu et al. 2016) Though JE pith powders are born with dye adsorption ability, there still have two questions. The adsorption capacity is not good enough as well as it difficult to be separated from water because its density being small and difficult to collect. In this paper, we focused on these two questions and proposed the solutions. The citric acid-modified JE pith powders loaded with Fe_3O_4 nanoparticles (M-CA/JEPP) were prepared to serve as an easily separated green adsorbent for MB adsorption. To our best of knowledge, there were barely reports about the citric acid-modified magnetic dye adsorbents based on biomass. The effects of different factors, such as pH, contact time and temperature on the adsorption performance were systematically evaluated, and the parameters of adsorption isotherms, thermodynamics and kinetics were obtained by fitting with classical models. Furthermore, the adsorption mechanism was also proposed based on the experiment. In all, M-CA/JEPP is a novel high performance cellulose-based magnetic adsorbents with excellent reusability and separation ability from wastewater. It may open the window for development of green adsorbents to remove dye in wastewater treatment.

Experimental Section

Materials

Dry Juncus effusus pith powders (JEPP) were purchase from the local Chinese herb shop. Sodium hydroxide (NaOH) and citric acid (CA) were obtained from Shanghai Ling Feng Chemical Reagent Co., Ltd. Ferric trichloride ($FeCl_3·6H_2O$), ferrous sulfate ($FeSO_4·7H_2O$) and hydrochloric acid (HCl) were purchased from Sinopharm Chemical Reagent Co., Ltd. Ammonia solution ($NH_3·H_2O$, 25-28 wt%) was purchase from Shanghai Macklin Biochemical Co., Ltd. Methylene Blue (MB) was purchased from J&K Scientific Ltd.

Synthesis methods

Preparation of CA-modified JEPP (CA/JEPP)

Prior to CA modification, dry JEPP were screened using a 100 mesh sieve. Then 9 g of JEPP were added to 180 mL of 0.1 M NaOH solution, this alkali treatment was stirred at 65 ℃ for 1 h. After cooling to room temperature, the pre-treated JEPP were rinsed with deionized water until the pH of the filtrate dropped to neutral. Water was drained and the washed JEPP were dried in an oven at 50 ℃ for 24 h.

The esterification modification by CA was as follows: Briefly, 1.1 g of as-prepared JEPP were added to 11 mL of 0.6 M CA at room temperature with stirring for 30 min. After draining the liquid, the wet powders were placed in an oven at 50 ℃ for 24 h. Then the temperature of the oven was raised to 120 ℃, and this temperature was kept for 90 min. The modified JEPP were washed several times using hot deionized water about 70 °C to remove excess citric acid. The wet powders are placed in an oven at 50 ℃ for 24 h, the dry products named CA/JEPP were milled and stored in a desiccator.

Synthesis of CA-modified magnetic JEPP (M-CA/JEPP)

The magnetic adsorbent M-CA/JEPP-1 was synthesized by a facile co-precipitation method that did not require an inert atmosphere. (Mahdavinia et al. 2016) 1.081 g of $FeCl_3 \cdot 6H_2O$ (2.5 mmol) and 0.695 g of $FeSO_4 \cdot 7H_2O$ (4.0 mmol) were dissolved in 100 mL distilled water to obtain a brownish-yellow mixed solution. 0.926 g of the CA/JEPP were added to the iron ions solution and stirred for 20 min at room temperature. Afterward, 20 mL of ammonia solution (25-28 wt%) was slowly dropped into the mixture with ultrasonic oscillations. The reaction was placed in a water bath at 70 ℃ and stirred for 1 h. After cooling the mixture to room temperature, the magnetic products were separated by magnet and washed with ethanol-water mixture for several times. Finally, the M-CA/JEPP were obtained after vacuum drying at 60 °C for 6 h. The different doses of $FeSO_4 \cdot 7H_2O$ and $FeCl_3 \cdot 6H_2O$ were used to obtain M-CA/JEPP-2 and M-CA/JEPP-3. More information was shown in **Table S1** and **Fig. S1.** M-CA/JEPP-1 was selected as the most effective adsorbent and re-named as M-CA/JEPP which was further used in the following experiments.

Characterization

The fourier transforms infrared spectroscopy (FTIR) analysis of the samples were performed on a FTIR spectrometer (Nicolet IS50, Thermo Fisher Scientific, USA) at room temperature in the range of 4000-400 cm^{-1}. X-ray diffraction measurements were tested on an X-ray diffractometer (XRD, D8 Advance Bruker, Germany) using Cu Kα radiation in the range of 2θ=5-80° with a scanning rate of 10 °/min. The X-ray photoelectron spectroscopy (XPS) spectra were carried out by a Thermo Scientific K-Alpha with a monochromatic source of X-rays (Al Kα, hv=1486.6 eV). The morphologies of JEPP and M-CA/JEPP were observed on a Field emission scanning electron microscopy (FE-SEM, Sigma300, ZEISS, Germany) and energy dispersive spectroscopy (EDS) coupled with SEM was used. The particle size and distribution of Fe_3O_4 loaded on the adsorbent were analyzed by transmission electron microscopy (TEM, TF20, Thermo Fisher Scientific, USA). Magnetic properties were obtained using a vibrating sample magnetometer LakeShore7404 (VSM, LakeShore, USA) at room temperature. The specific surface area of the sample

was. characterized by Brunauer-Emmett-Teller (BET) tests using a specific surface area and porosity analyzer (ASAP2460, Micromeritics, USA).

Batch adsorption experiments

Dry magnetic adsorbents were used for adsorption experiments. Typically, 10 mg of M-CA/JEPP were added into 20 mL of MB dye solution of known concentration at certain temperature, followed by shaking in a water bath shaker at 200 rpm. After adsorption, the adsorbents were separated from mixture by a magnet. The residual concentration of MB was determined by a UV visible spectrophotometer (UV-2550, Shimadzu, Japan) at 664 nm. Each experiment was carried out in triplicate. The amount of dye adsorbed at time t (q_t) (mg/g) or at equilibrium (q_e) (mg/g) and the adsorption efficiency (%) were calculated using **Equation 1-3**:

$$q_t = \frac{(C_0 - C_t)V}{m} \quad (1)$$

$$q_e = \frac{(C_0 - C_e)V}{m} \quad (2)$$

$$\text{adsorption efficiency} = \frac{(C_0 - C_e)}{C_0} \times 100\% \quad (3)$$

where C_0, C_e and C_t (mg/L) are the initial, at time t and equilibrium concentration of dye solution, respectively, V (L) is the volume of solution, and m (g) is the mass of the adsorbent.

For the initial pH impact study, 10 mg of M-CA/JEPP were added into a flask containing 20 ml of MB solution (100 mg/L) at different initial pH, ranging from pH 4 to 11. The initial pH was adjusted with 0.1 M HCl or 0.1 M NaOH. In order to evaluate the effect of initial dye concentration on adsorption, various dye solution containing 100-500 mg/L of MB were prepared for adsorption. The concentration of MB during adsorption process were measured at predetermined time intervals to study the influence of contact time. Adsorption kinetics, isotherms and thermodynamics were also conducted to investigate the adsorption performance and mechanisms.

Reusability experiments

After adsorption (initial dye concentration was 50 mg/L), 10 mg of adsorbents were separated by a magnet and regenerated with 10 mL of 0.1 M HCl in a rotary shaker at 200 rpm for 20 minutes at 30 °C. Then the adsorbent was rinsed several times using deionized water and was placed in a vacuum oven at 60 °C for 6 h to obtain the regenerated adsorbent. The regenerated adsorbent was added to 50 mg/L MB solution again as the next adsorption cycle. And the reusability of M-CA/JEPP was performed as described above for five cycles.

Results And Discussion

Preparation of M-CA/JEPP

The synthesis of magnetic bio-adsorbent M-CA/JEPP derived from Juncus effusus was illustrated in Scheme 1. Dry JEPP were washed by alkali to remove contaminants and reduce hemicelluloses and lignin contents. (Xia et al. 2019) Then citric acid was dehydrated to obtain anhydride under 120 ℃ and combined with the hydroxyl groups in the cellulose to form an ester linkage to endowed the biomass with carboxyl groups. (Sajab et al. 2013; Zhu et al. 2008) Finally, the magnetic particles were loaded on cellulose by chemical co-precipitation to fabrication the adsorbent.

Chemical structure and morphology characterization of M-CA/JEPP

The functional groups of JEPP, CA/JEPP and M-CA/JEPP and their positions were determined by FTIR. As shown in Fig. 1a, a broad peaks between 3000–3700 cm^{-1} was linked to -OH stretching vibrations involved in the hydrogen bond interaction. (Lu et al. 2021) The absorption peaks observed at 2922 cm^{-1} and 2848 cm^{-1} corresponded to C-H stretching vibrations from CH and CH_2 in cellulose, hemicellulose and lignin. Similarly, multiple peaks in the regions between 1000–1800 cm^{-1} were related to the functional groups in cellulose, hemicellulose and lignin of the plant. Among them, the peak centered at 1736 cm^{-1} was attributable to the C = O stretching of hemicelluloses, the peak located at 1513 cm^{-1} was associated with C = C groups from lignin and the peak around 1250 cm^{-1} came from C–O stretching in lignin and hemicelluloses. (Maache et al. 2017; N et al. 2018; Xia et al. 2019) The peaks of CA/JEPP near 1250 cm^{-1} and 1513 cm^{-1} were dramatically reduced, indicating a decrease in lignin and hemicellulose, which may be due to the alkali treatment, while a significant enhancement of the peak at 1736 cm^{-1} could prove that citric acid have reacted with cellulose successfully. After magnetizing, the visible peak of M-CA/JEPP around 580 cm^{-1} belonged to Fe-O bonds in Fe_3O_4, and the peak appeared at 1400 cm^{-1} indicated the presence of COO^-. The peak of C = O vibration from citric acid moved from 1736 cm^{-1} to 1613 cm^{-1} because of the influence of covalent bonds on the surface of Fe_3O_4, (Ashour et al. 2017) implying the interaction existed in Fe_3O_4 and citric acid.

The X-ray diffraction patterns were conducted to identify the crystal structure of JEPP and M-CA/JEPP (Fig. 1b). Weak and broad peaks of the origin JEPP around 16.7° and 22.6° represented the amorphous

region and crystalline area of cellulose. (Xia et al. 2019) The XRD pattern of M-CA/JEPP exhibited the typical diffraction peaks of trans spinel structure which was consistent with Fe_3O_4. The characteristic peaks at 30.2°, 35.5°, 43.2°, 53.7°, 57.1° and 62.7° were attributed to (220), (311), (400), (422), (511), (440) crystal planes, respectively. (Gupta and Nayak 2012)

To analyze the chemical composition and electronic states of various elements, XPS analysis was also performed and the results were compiled in Fig. 1c-f. The presence of carbon, oxygen, and iron peaks was confirmed by the XPS wide-scan survey of M-CA/JEPP (Fig. 1c). In the high-resolution XPS spectrum for C1s (Fig. 1d), there were three peaks located at 284.8 eV, 286.5 eV, and 288.1 eV attributing to C-C, C-O, and C = O/O = C-O, (Yuan et al. 2019) respectively. The high-resolution XPS spectrum for O1s (Fig. 1e) could be deconvoluted into four individual peaks around 530.0 eV, 531.3 eV, 532.8 eV and 533.1 eV which was corresponded to Fe-O, C = O/O = C-O, O-H, and C-O, (Li et al. 2011; Yuan et al. 2019) respectively. The Fe2p spectrum (Fig. 1f) showed two main peaks at 710.3 and 724.9 eV, which could be assigned as $Fe2p_{3/2}$ and $Fe2p_{1/2}$ from Fe_3O_4 (Sitthichai et al. 2015) The deconvoluted peaks of Fe2p spectrum were linked to octahedral Fe^{3+} species, tetrahedral Fe^{3+} species, satellite peak of Fe^{3+} and Fe^{2+} ions, and octahedral Fe^{2+} species. (Lu et al. 2018; Wilson and Langell 2014) Combined the results of FTIR, XRD and XPS, it could indicate that magnetic Fe_3O_4 was synthesized and incorporated into the CA-modified JEPP successfully.

The microstructure and surface morphology of initial JEPP and M-CA/JEPP were characterized by SEM. As shown in Fig. 2a, JEPP presented the shape of framing scaffold structure and smooth surface. Micro pores could be observed on the framing scaffold structure which were several microns in size. After modification and magnetizing, the surface of obtained M-CA/JEPP became extremely rough with the large pores disappeared, but some cracks and pits which might be conducive to adsorption were formed (Fig. 2b, d, e). The EDS spectra of M-CA/JEPP (Fig. 2c) only exhibited the peaks of C, O, and Fe, which were three major constituents of CA-modified fibers and magnetite, confirming there hasn't impurities introduced during the synthesis process. Additionally, Fig. 2e showed there were plenty of magnetic nanoparticles covering on the surface of modified JEPP and the specific surface area was 34.15 m^2/g (**Fig. S2**). Moreover, the EDS mapping were performed (Fig. 2f). The resulting patterns showed that C, O, Fe elements were uniformly distributed throughout the adsorbent powders, which was strong evidence for the combination of Fe_3O_4 and CA/JEPP.

The size and distribution of magnetic nanoparticles on adsorbents were shown in TEM images (**Fig. S3a, b**). The Fe_3O_4 nanoparticles were evenly distributed on the surface of the powders, whose average size was 6.60 nm (**Fig. S3d**). There was no serious aggregation between those nanoparticles. The ultrasonic assistance and citric acid modification in the fabrication process could reduce the possibility of aggregation and was beneficial for better dispersion. (Liu et al. 2009) As presented in high-resolution transmission electron microscopy (HRTEM) image (**Fig. S3c**), the lattice fringes of the samples displayed interplanar spacings of 0.254 nm and 0.302 nm in the nanoparticles, which matched well respectively with the (311) and the (220) characteristic lattice planes of Fe_3O_4. (Alqadami et al. 2017)

Adsorption properties of the adsorbent

Effects of initial pH on MB adsorption

The initial pH value of the dye solution is a significant influencing factor for adsorption performance. Alkaline conditions were conducive to the adsorption of MB dyes by M-CA/JEPP. It could be seen from Fig. 3a that the adsorption efficiency of MB was gradually enhanced with pH increasing from 4 to 11. At pH 4, the adsorption efficiency of MB was 77.61%, while the adsorption efficiency of MB increased to 98.62% at pH 11. Similarly, Fig. 3b implied that the adsorption capacity was increased from 155.22 mg/g to maximum value (197.25 mg/g) while the pH was adding up from 4 to 11. Therefore, pH = 11 was chosen to study the adsorption properties in other experiments.

The pH of the solution will affect the dissociation of functional groups on the surface of M-CA/JEPP, which has a corresponding effect on the adsorption behavior. Under the acidic condition with low pH, more free hydrogen ions (H^+) in the solution competed with the cationic MB molecules to occupy the active site of the adsorbents, which inhibited the adsorption of MB. (Kausar et al. 2022) As the pH rose from 4 to 11, the numbers of OH^- ions in the solution increased, promoting the dissociation of H^+ ions which came from -OH and -COOH functional groups on the surface of M-CA/JEPP. The electronegativity of the adsorbent enhanced, and the adsorption efficiency and adsorption capacity became higher owing to the electrostatic attraction between cationic dye and adsorbents.

Effects of contact time on MB adsorption

The contact time between adsorbents and dyes always affects the final result of the adsorption. Figure 3c presented rapid adsorption of dye in the first 10 min, for MB dye solution with initial concentrations of 50 mg/L, 100 mg/L, 150 mg/L, the adsorption efficiency could reach 98.34%, 95.21%, 88.93%. Thereafter, the adsorption efficiency increased gradually, and the adsorption quickly reached equilibrium in around 60 min. With increasing of initial dye concentration, the adsorption capacity could reach up to a higher equilibrium value with time increasing (Fig. 3d). But the increased in contact time has promoted the aggregation of dye molecules, (Kumar et al. 2010) which made it almost impossible to diffuse deeper into the adsorbent structure and hindered the unlimited increasing of adsorption capacity.

Effects of initial dye concentration on MB adsorption

The effect of initial dye concentration in the range of 10 to 500 mg/L was investigated and the results were shown in Fig. 3e, f. As the initial dye concentration increased, the adsorption efficiency declined (Fig. 3e). While the adsorption efficiency for MB was found to be 98.62% for 100 mg/L of initial concentration, the value was 28.82% with the initial dye concentration was 500 mg/L. As shown in Fig. 3f, the adsorption capacity increased and finally tend to be stable with the initial dye concentration increasing. Since high initial dye concentration might provide the high driving force for the mass transfer, (Salleh et al. 2011) the adsorption capacity increased from 197.25 mg/g to 272.08 mg/g with the initial dye concentration changed from 100 mg/L to 150 mg/L. However, as the adsorbent dose was fixed, which

meant the available active sites were limited, so the adsorption capacity would become similar if the initial dye concentration was higher than 150 mg/L.

Magnetic property and reusability of M-CA/JEPP

The M-CA/JEPP showed powerful magnetic property. The magnetization curve in Fig. 4a revealed the ferromagnetic behavior of M-CA/JEPP, its saturation magnetization was 24.8 emu/g, which was significantly stronger than 3.6 emu/g (Gao et al. 2019) and 5.0 emu/g (Zhou et al. 2021) in other magnetic cellulose-based adsorbent works. Therefore, this new type of adsorbent showed powerful magnetic responsivity, and it could be separated conveniently within ten seconds from the treated solution with the help of an external magnetic force (Fig. 4b). In other words, it can be used as a magnetic trigger to finish the separation and reuse process in wastewater treatment.

The cyclic adsorption experiment was performed to investigate the regeneration of the adsorbent (Fig. 4c). The adsorbent was regenerated by using 0.1 M HCl as desorption reagent after adsorption. The results showed that for 50 mg/L MB solution, the removal efficiency of the M-CA/JEPP towards MB could maintain a level above 98% after five cycles, which was hardly reduced, suggesting that the adsorbent had outstanding recyclability.

Proposed adsorption mechanism

In order to explore the adsorption mechanism of MB dye by M-CA/JEPP, the infrared spectrum tests were carried out (Fig. 4d). The absorption peaks of 1300–1430 cm^{-1} and 1600 cm^{-1} showed that MB was combined with the adsorbents. For M-CA/JEPP, the peak of COO^- groups migrated from 1400 cm^{-1} to 1393 cm^{-1}, while the absorption peak of –OH functional groups at 3420 cm^{-1} moved to 3411 cm^{-1}, indicating that the adsorption process involved electrostatic adsorption and hydrogen bonding. (Liu et al. 2015; Meng et al. 2022) In addition, the role of pores and the π-π interaction between the benzene ring in MB molecule and the hexagonal skeleton of adsorbent (Leng et al. 2015) might also make important contributions to the adsorption (**Scheme 2**).

Scheme 2 Schematic drawing of recycling and the possible adsorption mechanism of M-CA/JEPP towards MB

Fitting results of the adsorption process

Adsorption kinetics

Four typical kinetic models including pseudo-first-order, pseudo-second-order, Elovich and intraparticle diffusion were conducted to calculate the rate constants and other parameters of the M-CA/JEPP for MB adsorption according to **Equation S1-S4**. The fitting results and parameters were shown in Fig. 5 and Table 1.

The correlation coefficient (R^2) was used to assess the degree of conformity between the experimental values and the theoretical values of the model. According to the fitting results of different concentrations

of MB, the R^2 values calculated by the pseudo-first-order dynamic model were between 0.969–0.989. The R^2 values of the intraparticle diffusion model were between 0.577–0.977, and its fitted line were not zeroaxial, which indicated that intraparticle diffusion was not the rate-limiting step of the whole adsorption. (Peng et al. 2021) Elovich model was commonly used to deal with the chemical adsorption mechanism in nature, the R^2 values of Elovich model were in the range of 0.935–0.975. (Shahnaz et al. 2022) The R^2 values calculated by the pseudo-second-order dynamic model were above 0.996 and the obtained $q_{e,cal}$ values were also closest to the original experimental values. So pseudo-second-order model was more appropriate for defining this adsorption process, suggesting that the rate control step occurred during the entire adsorption process. (Li et al. 2021)

Table 1
Kinetic parameters for different initial concentrations of MB on M-CA/JEPP with various models

Kinetics models	Parameters	Initial concentration		
		50 mg/L	100 mg/L	150 mg/L
Pseudo-first-order	$q_{e,exp}$ (mg/g)	98.837	197.247	276.450
	$q_{e,cal}$ (mg/g)	97.678	192.348	267.360
	k_1 (min^{-1})	2.298	0.851	1.554
	R^2	0.989	0.986	0.969
Pseudo-second-order	$q_{e,exp}$ (mg/g)	98.837	197.247	276.450
	$q_{e,cal}$ (mg/g)	99.783	200.526	275.755
	k_2 [g/(mg min)]	0.050	0.006	0.010
	R^2	0.999	0.999	0.996
Elovich	α [mg/g min]	1.667E + 9	7.482E + 3	8.630E + 5
	β [g/mg]	0.237	0.049	0.053
	R^2	0.974	0.935	0.975
Intrapaticle diffusion	$k_{p,1}$ [mg/g $min^{-0.5}$]	29.089	95.758	86.421
	C_1 (mg/g)	51.373	12.256	107.896
	R^2	0.997	0.965	0.992
	$k_{p,2}$ [mg/g $min^{-0.5}$]	0.166	1.886	2.742
	C_2 (mg/g)	97.641	180.751	253.277
	R^2	0.938	0.577	0.649

Adsorption isotherm

Langmuir, Freundlich and Temkin adsorption isotherms were used to explain the relationship between the adsorbent and adsorbate according to **Equation S5-S7**. The fitting results and parameters were shown in Fig. 6 and Table 2.

The results of the MB adsorption experiment at different temperatures indicated that the increase in temperature will make the adsorption capacity lower. Langmuir isotherm model was the most suitable model, whose R^2 values were above 0.982. The maximum adsorption capacity of M-CA/JEPP for MB at 303 K was 293.132 mg/g, which surpass many cellulosic adsorbents derived from biomass **(Fig. S4)**. The Langmuir isotherm is often used to describe monolayer adsorption on uniform surfaces, which is also based on the assumption that the adsorption energy at each point of the surface is the same and there is no interaction between the adsorbate molecules attached to the surface. The Freundlich isotherm which suppose the energy on the surface is uneven is often used to describe multilayer adsorption. Furthermore, The Temkin isotherms assume that the adsorption heat of all molecules in the layer will decrease linearly with coverage rate due to the adsorbent/adsorbent interaction, which is commonly used to explain the interaction between adsorbent molecules adsorbed on the surface. (Eslek Koyuncu and Okur 2021; Tan et al. 2007) The optimal adaptation of the Langmuir isotherm substantiated that the MB adsorption by M-CA/JEPP was monolayer adsorption rather than multilayer adsorption. In addition, one essential characteristic of the Langmuir isotherm could be expressed by the separation factor R_L calculated from **Equation S8**. In the present study, R_L values were between 0–1, indicating that the adsorption process under experimental conditions is conducive to proceeding. (Wibowo et al. 2017)

Table 2
Isotherm parameters for MB on M-CA/JEPP with various models at different temperature

Isotherm models	Parameters	Temperature		
		303 K	313 K	323 K
Langmuir	q_{max} (mg/g)	293.132	284.929	279.584
	k_l (L/mg)	1.124	1.159	1.076
	R^2	0.986	0.982	0.992
Freundlich	*1/n*	0.154	0.154	0.156
	k_f [(mg/g)/(mg/L)$^{1/n}$]	133.957	130.151	126.474
	R^2	0.782	0.787	0.813
Temkin	*B*	33.578	32.440	31.948
	A_T (L/g)	46.887	48.667	47.059
	R^2	0.876	0.876	0.903

Adsorption thermodynamic.

After the experimental data fitted by **Equation S9-S11**, the thermodynamic parameters (Gibbs free energy change (ΔG), enthalpy change (ΔH), entropy change (ΔS) of this adsorption process could be calculated, the fitting lines and the calculated results were displayed in **Fig. S5** and **Table S2**. Among the results, $\Delta G < 0$ proved that the adsorption was a spontaneous process. The Negative ΔH indicated that these processes were exothermic, which further confirmed that temperature increasing was not beneficial for the adsorption. $\Delta S > 0$ suggested that due to the increased randomness of the solution/solid interface, adsorbent/adsorbent composites are formed. (Chen et al. 2015; Yu et al. 2019) Moreover, ΔH was between 0–84 kJ/mol, which meant this MB adsorption process could be mainly regarded as physical adsorption. (Errais et al. 2011)

Conclusion

In summary, we have demonstrated a simple approach to obtain CA-modified magnetic cellulose-based adsorbent. Compared with original JEPP, M-CA/JEPP had a rougher surface and richer functional groups, so its adsorption performance was greatly improved. The adsorption process was proved to be a spontaneous and exothermic reaction, where the adsorption data fitted the Langmuir isotherm and the pseudo-second-order model well. It could quickly reach the adsorption equilibrium within tens of minutes, with a maximum adsorption capacity of 293.132 mg/g for MB at 303 K. The superior adsorption performance of M-CA/JEPP might be mainly attributed to electrostatic interaction and hydrogen bonding. Furthermore, this kind of adsorbents was easy to recycle with magnet and could maintain preeminent reusability in five cycles, which was more in line with the requirements of environmental protection. These findings will expand our horizons for preparing cellulosic adsorbents from nature to deal with dye contamination in aqueous system.

Declarations

Ethics approval and consent to participate

Not applicable.

Consent for publication

Not applicable.

Availability of data and materials

The datasets used and analyzed during the current study available from the corresponding author on reasonable request.

Author contributions

All authors contributed to the study conception and design. Material preparation, data collection and analysis were performed by Keming Zhou. The first draft of the manuscript was written by

Keming Zhou and all authors commented on previous versions of the manuscript. All authors read and approved the final manuscript.

Funding

This work was supported by the National Natural Science Foundation of China (21374029, 21776076), Open Research Fund of Shanghai Key Laboratory of Green Chemistry and Chemical Processes, East China Normal University and Fundamental Research Funds for the Central Universities (JKA01221712).

Competing interests

The authors have no relevant financial or non-financial interests to disclose.

Acknowledgments

This work is supported by the National Natural Science Foundation of China (21374029, 21776076) and the Open Research Fund of Shanghai Key Laboratory of Green Chemistry and Chemical Processes, East China Normal University. We also thank Fundamental Research Funds for the Central Universities (JKA01221712).

References

1. Ahsan MA, Jabbari V, Imam MA, Castro E, Kim H, Curry ML, Valles-Rosales DJ, Noveron JC (2020) Nanoscale nickel metal organic framework decorated over graphene oxide and carbon nanotubes for water remediation. Sci Total Environ 698:134214. https://doi.org/10.1016/j.scitotenv.2019.134214
2. Aliabadi RS, Mahmoodi NO (2018) Synthesis and characterization of polypyrrole, polyaniline nanoparticles and their nanocomposite for removal of azo dyes; sunset yellow and Congo red. *J Clean Prod* 179:235-245. https://doi.org/10.1016/j.jclepro.2018.01.035
3. Aljerf L (2018) High-efficiency extraction of bromocresol purple dye and heavy metals as chromium from industrial effluent by adsorption onto a modified surface of zeolite: Kinetics and equilibrium study. J Environ Manage 225:120-132. https://doi.org/10.1016/j.jenvman.2018.07.048
4. Alqadami AA, Naushad M, Alothman ZA, Ghfar AA (2017) Novel Metal-Organic Framework (MOF) Based Composite Material for the Sequestration of U(VI) and Th(IV) Metal Ions from Aqueous Environment. ACS Appl Mater Interfaces 9:36026-36037. https://doi.org/10.1021/acsami.7b10768
5. Alsbaiee A, Smith BJ, Xiao LL, Ling YH, Helbling DE, Dichtel WR (2016) Rapid removal of organic micropollutants from water by a porous beta-cyclodextrin polymer. Nature 529:190-194. https://doi.org/10.1038/nature16185
6. Alver E, Metin AÜ (2012) Anionic dye removal from aqueous solutions using modified zeolite: Adsorption kinetics and isotherm studies. Chem Eng J 200-202:59-67. https://doi.org/10.1016/j.cej.2012.06.038

7. Ashour RM, El-sayed R, Abdel-Magied AF, Abdel-khalek AA, Ali MM, Forsberg K, Uheida A, Muhammed M, Dutta J (2017) Selective separation of rare earth ions from aqueous solution using functionalized magnetite nanoparticles: kinetic and thermodynamic studies. Chem Eng J 327:286-296. https://doi.org/10.1016/j.cej.2017.06.101
8. Bhatia D, Sharma NR, Singh J, Kanwar RS (2017) Biological methods for textile dye removal from wastewater: A review. Crit Rev Environ Sci Technol 47:1836-1876. https://doi.org/10.1080/10643389.2017.1393263
9. Brillas E, Martínez-Huitle CA (2015) Decontamination of wastewaters containing synthetic organic dyes by electrochemical methods. An updated review. Appl Catal B 166-167:603-643. https://doi.org/10.1016/j.apcatb.2014.11.016
10. Chen H, Wang XX, Li JX, Wang XK (2015) Cotton derived carbonaceous aerogels for the efficient removal of organic pollutants and heavy metal ions. J Mater Chem A 3:6073-6081. https://doi.org/10.1039/c5ta00299k
11. Chen HF, Zhou Y, Wang JY, Lu J, Zhou YB (2020) Polydopamine modified cyclodextrin polymer as efficient adsorbent for removing cationic dyes and Cu(II). J Hazard Mater 389:121897. https://doi.org/10.1016/j.jhazmat.2019.121897
12. Chen LW, Zhu YY, Cui YM, Dai R, Shan ZH, Chen H (2021) Fabrication of starch-based high-performance adsorptive hydrogels using a novel effective pretreatment and adsorption for cationic methylene blue dye: Behavior and mechanism. Chem Eng J 405:126953. https://doi.org/10.1016/j.cej.2020.126953
13. Crini G, Lichtfouse E (2018) Advantages and disadvantages of techniques used for wastewater treatment. *Environ Chem Lett* 17:145-155. https://doi.org/10.1007/s10311-018-0785-9
14. Cseri L, Topuz F, Abdulhamid MA, Alammar A, Budd PM, Szekely G (2021) Electrospun Adsorptive Nanofibrous Membranes from Ion Exchange Polymers to Snare Textile Dyes from Wastewater. Adv Mater Technol *2000955.* https://doi.org/10.1002/admt.202000955
15. Değermenci GD, Değermenci N, Ayvaoğlu V, Durmaz E, Çakır D, Akan E (2019) Adsorption of reactive dyes on lignocellulosic waste; characterization, equilibrium, kinetic and thermodynamic studies. J Clean Prod 225:1220-1229. https://doi.org/10.1016/j.jclepro.2019.03.260
16. Errais E, Duplay J, Darragi F, M'Rabet I, Aubert A, Huber F, Morvan G (2011) Efficient anionic dye adsorption on natural untreated clay: Kinetic study and thermodynamic parameters. Desalination 275:74-81. https://doi.org/10.1016/j.desal.2011.02.031
17. Eslek Koyuncu DD, Okur M (2021) Removal of AV 90 dye using ordered mesoporous carbon materials prepared via nanocasting of KIT-6: Adsorption isotherms, kinetics and thermodynamic analysis. Sep Purif Technol 257:117657. https://doi.org/10.1016/j.seppur.2020.117657
18. Gao HJ, Du J, Liao YW (2019) Removal of chromium(VI) and orange II from aqueous solution using magnetic polyetherimide/sugarcane bagasse. Cellulose 26:3285-3297. https://doi.org/10.1007/s10570-019-02301-7

19. Gong RM, Jin YB, Chen FY, Chen J, Liu ZL (2006) Enhanced malachite green removal from aqueous solution by citric acid modified rice straw. J Hazard Mater 137:865-870. https://doi.org/10.1016/j.jhazmat.2006.03.010
20. Gong RM, Zhu SX, Zhang DM, Chen J, Ni SJ, Guan R (2008) Adsorption behavior of cationic dyes on citric acid esterifying wheat straw: kinetic and thermodynamic profile. Desalination 230:220-228. https://doi.org/10.1016/j.desal.2007.12.002
21. Gupta VK, Nayak A (2012) Cadmium removal and recovery from aqueous solutions by novel adsorbents prepared from orange peel and Fe_2O_3 nanoparticles. Chem Eng J 180:81-90. https://doi.org/10.1016/j.cej.2011.11.006
22. Han XL, Wang W, Ma XJ (2011) Adsorption characteristics of methylene blue onto low cost biomass material lotus leaf. *Chem Eng J* 171:1-8. https://doi.org/10.1016/j.cej.2011.02.067
23. Jawad AH, Abdulhameed AS, Reghioua A, Yaseen ZM (2020) Zwitterion composite chitosan-epichlorohydrin/zeolite for adsorption of methylene blue and reactive red 120 dyes. Int J Biol Macromol 163:756-765. https://doi.org/10.1016/j.ijbiomac.2020.07.014
24. Jiang N, Shang R, Heijman SGJ, Rietveld LC (2018) High-silica zeolites for adsorption of organic micro-pollutants in water treatment: A review. Water Res 144:145-161. https://doi.org/10.1016/j.watres.2018.07.017
25. Kausar A, Rehman SU, Khalid F, Bonilla-Petriciolet A, Mendoza-Castillo DI, Bhatti HN, Ibrahim SM, Iqbal M (2022) Cellulose, clay and sodium alginate composites for the removal of methylene blue dye: Experimental and DFT studies. Int J Biol Macromol 209:576-585. https://doi.org/10.1016/j.ijbiomac.2022.04.044
26. Kumar PS, Ramalingam S, Senthamarai C, Niranjanaa M, Vijayalakshmi P, Sivanesan S (2010) Adsorption of dye from aqueous solution by cashew nut shell: Studies on equilibrium isotherm, kinetics and thermodynamics of interactions. Desalination 261:52-60. https://doi.org/10.1016/j.desal.2010.05.032
27. Leng LJ, Yuan XZ, Huang HJ, Shao JG, Wang H, Chen XH, Zeng GM (2015) Bio-char derived from sewage sludge by liquefaction: Characterization and application for dye adsorption. Appl Surf Sci 346:223-231. https://doi.org/10.1016/j.apsusc.2015.04.014
28. Li H, Li MJ, Zheng F, Wang J, Chen L, Hu PF, Zhen Q, Bashir S, Liu JL (2021) Efficient removal of water pollutants by hierarchical porous zeolite-activated carbon prepared from coal gangue and bamboo. J Clean Prod 325:129322. https://doi.org/10.1016/j.jclepro.2021.129322
29. Li JX, Chen SY, Sheng GD, Hu J, Tan XL, Wang XK (2011) Effect of surfactants on Pb(II) adsorption from aqueous solutions using oxidized multiwall carbon nanotubes. Chem Eng J 166:551-558. https://doi.org/10.1016/j.cej.2010.11.018
30. Li ZC, Hanafy H, Zhang L, Sellaoui L, Schadeck Netto M, Oliveira MLS, Seliem MK, Luiz Dotto G, Bonilla-Petriciolet A, Li Q (2020) Adsorption of congo red and methylene blue dyes on an ashitaba waste and a walnut shell-based activated carbon from aqueous solutions: Experiments,

characterization and physical interpretations. Chem Eng J 388:124263. https://doi.org/10.1016/j.cej.2020.124263

31. Liu FT, Lu R, Pan QM (2016) Juncus Pith: A Versatile Material for Automatic and Continuous Separation of Various Oil–Water Mixtures. ACS Sustain Chem Eng 5:922-928. https://doi.org/10.1021/acssuschemeng.6b02232
32. Liu J, Sun ZK, Deng YH, Zou Y, Li CY, Guo XH, Xiong LQ, Gao Y, Li FY, Zhao DY (2009) Highly water-dispersible biocompatible magnetite particles with low cytotoxicity stabilized by citrate groups. Angew Chem Int Ed Engl 48:5875-5879. https://doi.org/10.1002/anie.200901566
33. Liu L, Gao ZY, Su XP, Chen X, Jiang L, Yao JM (2015) Adsorption Removal of Dyes from Single and Binary Solutions Using a Cellulose-based Bioadsorbent. ACS Sustain Chem Eng 3:432-442. https://doi.org/10.1021/sc500848m
34. Lu BB, Bo YY, Yi MJ, Wang ZY, Zhang JC, Zhu ZY, Zhao YL, Zhang JH (2021) Enhancing the Solubility and Transdermal Delivery of Drugs Using Ionic Liquid-In-Oil Microemulsions. Adv Funct Mater 31:2102794. https://doi.org/10.1002/adfm.202102794
35. Lu JW, Fu FL, Zhang L, Tang B (2018) Insight into efficient co-removal of Se(IV) and Cr(VI) by magnetic mesoporous carbon microspheres: Performance and mechanism. Chem Eng J 346:590-599. https://doi.org/10.1016/j.cej.2018.04.077
36. Maache M, Bezazi A, Amroune S, Scarpa F, Dufresne A (2017) Characterization of a novel natural cellulosic fiber from Juncus effusus L. Carbohydr Polym 171:163-172. https://doi.org/10.1016/j.carbpol.2017.04.096
37. Mahdavinia GR, Mousanezhad S, Hosseinzadeh H, Darvishi F, Sabzi M (2016) Magnetic hydrogel beads based on PVA/sodium alginate/laponite RD and studying their BSA adsorption. Carbohydr Polym 147:379-391. https://doi.org/10.1016/j.carbpol.2016.04.024
38. Meng WL, Ma ZY, Shu JC, Li B, Su PX, Wang R, Chen MJ, Liu ZH, Ai KH (2022) Efficient adsorption of methylene blue from aqueous solution by hydrothermal chemical modification phosphorus ore flotation tailings. Sep Purif Technol 281:119496. https://doi.org/10.1016/j.seppur.2021.119496
39. N S, I R, T R (2018) Characterization of untreated and alkali treated new cellulosic fiber from an Areca palm leaf stalk as potential reinforcement in polymer composites. Carbohydr Polym 195:566-575. https://doi.org/10.1016/j.carbpol.2018.04.127
40. Paździor K, Bilińska L, Ledakowicz S (2019) A review of the existing and emerging technologies in the combination of AOPs and biological processes in industrial textile wastewater treatment. Chem Eng J 376:120597. https://doi.org/10.1016/j.cej.2018.12.057
41. Peng D, Cheng SP, Li HS, Guo XT (2021) Effective multi-functional biosorbent derived from corn stalk pith for dyes and oils removal. Chemosphere 272:129963. https://doi.org/10.1016/j.chemosphere.2021.129963
42. Sajab MS, Chia CH, Zakaria S, Khiew PS (2013) Cationic and anionic modifications of oil palm empty fruit bunch fibers for the removal of dyes from aqueous solutions. Bioresour Technol 128:571-577. https://doi.org/10.1016/j.biortech.2012.11.010

43. Salleh MAM, Mahmoud DK, Karim WAWA, Idris A (2011) Cationic and anionic dye adsorption by agricultural solid wastes: A comprehensive review. Desalination 280:1-13. https://doi.org/10.1016/j.desal.2011.07.019
44. Shahnaz T, Bedadeep D, Narayanasamy S (2022) Investigation of the adsorptive removal of methylene blue using modified nanocellulose. Int J Biol Macromol 200:162-171. https://doi.org/10.1016/j.ijbiomac.2021.12.081
45. Shannon MA, Bohn PW, Elimelech M, Georgiadis JG, Marinas BJ, Mayes AM (2008) Science and technology for water purification in the coming decades. Nature 452:301-310. https://doi.org/10.1038/nature06599
46. Shao XY, Wang J, Liu ZT, Hu N, Liu M, Duan C, Zhang RM, Quan CL (2021) Cellulose based cation-exchange fiber as filtration material for the rapid removal of methylene blue from wastewater. Cellulose 28:9355-9367. https://doi.org/10.1007/s10570-021-04103-2
47. Sitthichai S, Pilapong C, Thongtem T, Thongtem S (2015) CMC-coated Fe_3O_4 nanoparticles as new MRI probes for hepatocellular carcinoma. Appl Surf Sci 356:972-977. https://doi.org/10.1016/j.apsusc.2015.08.140
48. Sun L, Chen DM, Wan SG, Yu ZB (2015) Performance, kinetics, and equilibrium of methylene blue adsorption on biochar derived from eucalyptus saw dust modified with citric, tartaric, and acetic acids. Bioresour Technol 198:300-308. https://doi.org/10.1016/j.biortech.2015.09.026
49. Tan IAW, Hameed BH, Ahmad AL (2007) Equilibrium and kinetic studies on basic dye adsorption by oil palm fibre activated carbon. Chem Eng J 127:111-119. https://doi.org/10.1016/j.cej.2006.09.010
50. Tanyildizi MŞ (2011) Modeling of adsorption isotherms and kinetics of reactive dye from aqueous solution by peanut hull. Chem Eng J 168:1234-1240. https://doi.org/10.1016/j.cej.2011.02.021
51. Varghese AG, Paul SA, Latha MS (2018) Remediation of heavy metals and dyes from wastewater using cellulose-based adsorbents. Environ Chem Lett 17:867-877. https://doi.org/10.1007/s10311-018-00843-z
52. Verma AK, Dash RR, Bhunia P (2012) A review on chemical coagulation/flocculation technologies for removal of colour from textile wastewaters. J Environ Manage 93:154-168. https://doi.org/10.1016/j.jenvman.2011.09.012
53. Wang HF, Li ZC, Yahyaoui S, Hanafy H, Seliem MK, Bonilla-Petriciolet A, Luiz Dotto G, Sellaoui L, Li Q (2021) Effective adsorption of dyes on an activated carbon prepared from carboxymethyl cellulose: Experiments, characterization and advanced modelling. Chem Eng J 417:128116. https://doi.org/10.1016/j.cej.2020.128116
54. Wibowo E, Rokhmat M, Sutisna, Khairurrijal, Abdullah M (2017) Reduction of seawater salinity by natural zeolite (Clinoptilolite): Adsorption isotherms, thermodynamics and kinetics. Desalination 409:146-156. https://doi.org/10.1016/j.desal.2017.01.026
55. Wilson D, Langell MA (2014) XPS analysis of oleylamine/oleic acid capped Fe_3O_4 nanoparticles as a function of temperature. Appl Surf Sci 303:6-13. https://doi.org/10.1016/j.apsusc.2014.02.006

56. Wong S, Ngadi N, Inuwa IM, Hassan O (2018) Recent advances in applications of activated carbon from biowaste for wastewater treatment: A short review. J Clean Prod 175:361-375. https://doi.org/10.1016/j.jclepro.2017.12.059
57. Xia LJ, Zhang CH, Wang AM, Wang YL, Xu WL (2019) Morphologies and properties of Juncus effusus fiber after alkali treatment. Cellulose 27:1909-1920. https://doi.org/10.1007/s10570-019-02933-9
58. Yeamin MB, Islam MM, Chowdhury A-N, Awual MR (2021) Efficient encapsulation of toxic dyes from wastewater using several biodegradable natural polymers and their composites. J Clean Prod 291:125920. https://doi.org/10.1016/j.jclepro.2021.125920
59. Yu DY, Wang YJ, Wu MH, Zhang L, Wang LL, Ni HG (2019) Surface functionalization of cellulose with hyperbranched polyamide for efficient adsorption of organic dyes and heavy metals. J Clean Prod 232:774-783. https://doi.org/10.1016/j.jclepro.2019.06.024
60. Yuan DW, Cadien K, Liu Q, Zeng HB (2019) Adsorption characteristics and mechanisms of O-Carboxymethyl chitosan on chalcopyrite and molybdenite. J Colloid Interface Sci 552:659-670. https://doi.org/10.1016/j.jcis.2019.05.023
61. Zeng HJ, Yu ZX, Shao LY, Li XH, Zhu M, Liu YC, Feng XF, Zhu XM (2021) A novel strategy for enhancing the performance of membranes for dyes separation: Embedding PAA@UiO-66-NH_2 between graphene oxide sheets. Chem Eng J 403:126281. https://doi.org/10.1016/j.cej.2020.126281
62. Zhang WX, Yang Q, Luo QH, Shi LL, Meng SJ (2020) Laccase-Carbon nanotube nanocomposites for enhancing dyes removal. J Clean Prod 242:118425. https://doi.org/10.1016/j.jclepro.2019.118425
63. Zhao SX, Zhou TS (2016) Biosorption of methylene blue from wastewater by an extraction residue of Salvia miltiorrhiza Bge. Bioresour Technol 219:330-337. https://doi.org/10.1016/j.biortech.2016.07.121
64. Zhao XL, Wang XJ, Lou T (2021) Preparation of fibrous chitosan/sodium alginate composite foams for the adsorption of cationic and anionic dyes. J Hazard Mate*r* 403:124054. https://doi.org/10.1016/j.jhazmat.2020.124054
65. Zhou SJ, Xia LJ, Fu Z, Zhang CH, Duan XY, Zhang SY, Wang YL, Ding CL, Liu X, Xu WL (2021) Purification of dye-contaminated ethanol-water mixture using magnetic cellulose powders derived from agricultural waste biomass. Carbohydr Polym 258:117690. https://doi.org/10.1016/j.carbpol.2021.117690
66. Zhu B, Fan TX, Zhang D (2008) Adsorption of copper ions from aqueous solution by citric acid modified soybean straw. J Hazard Mater 153:300-308. https://doi.org/10.1016/j.jhazmat.2007.08.050

Scheme

Scheme 1 and 2 is available in the Supplementary Files section.

Figures

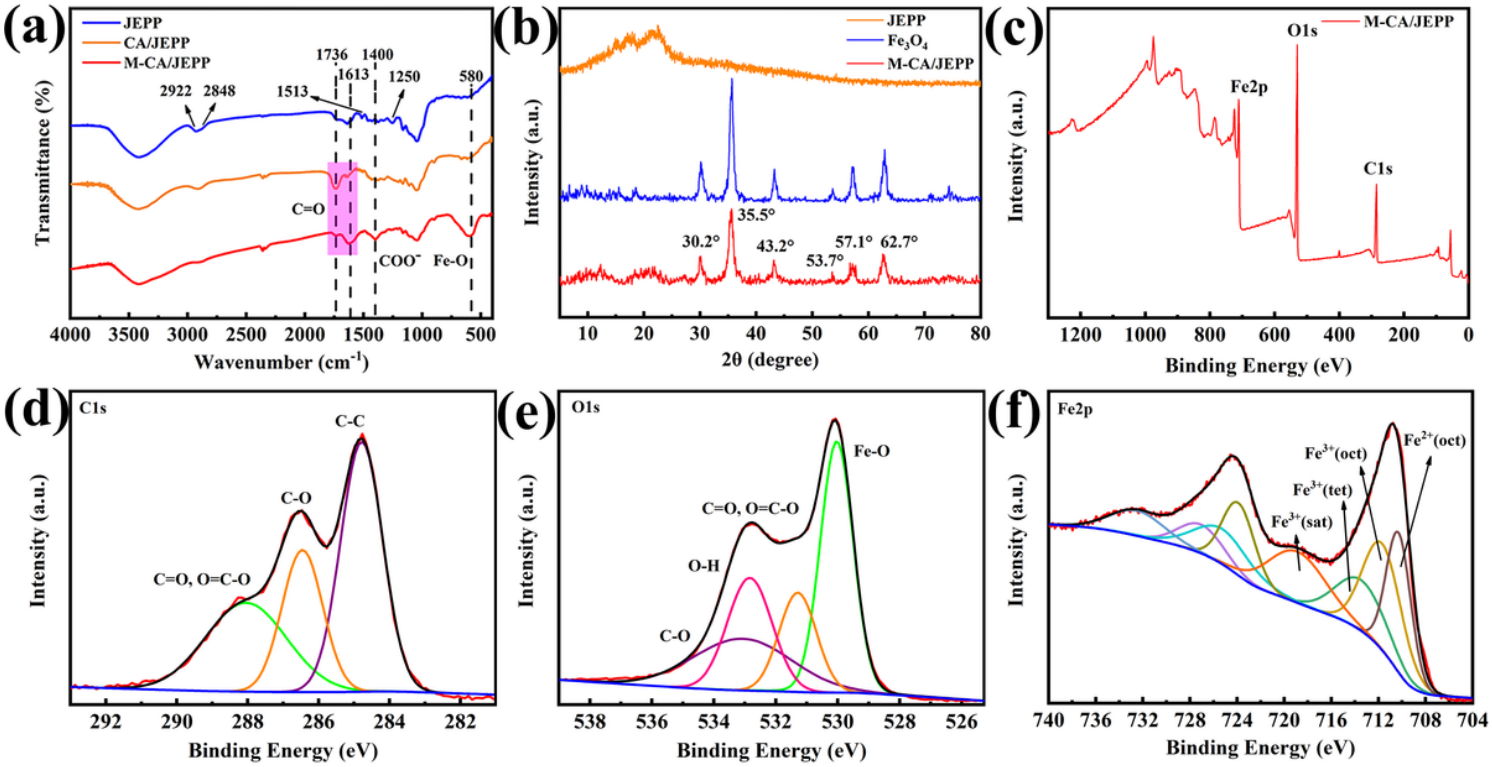


Figure 1

(a) FTIR spectra of JEPP, CA/JEPP and M-CA/JEPP. (b) XRD patterns of JEPP, Fe3O4 and M-CA/JEPP. (c) Wide-scan XPS spectra of M-CA/JEPP; High-resolution XPS spectra of (d) C1s, (e) O1s, (f) Fe2p for M-CA/JEPP

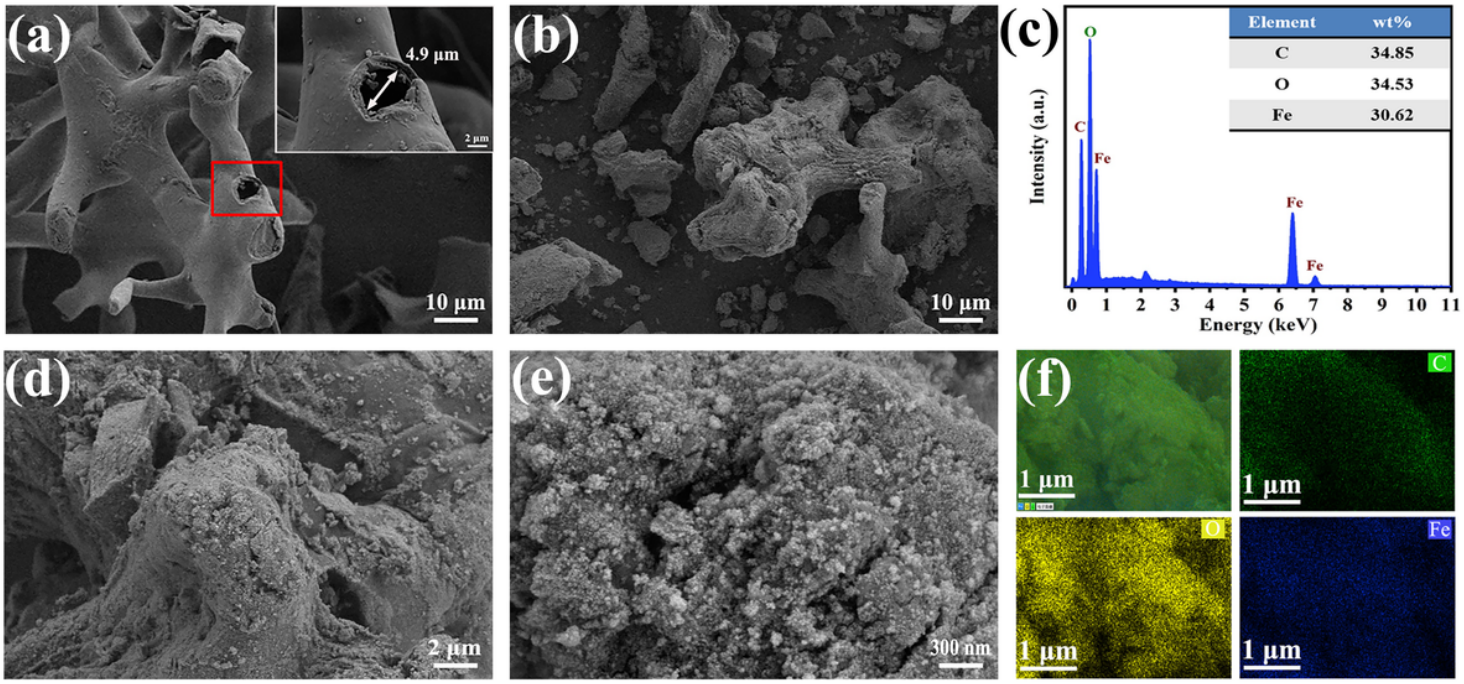


Figure 2

SEM images of (a) JEPP (b, d, e) M-CA/JEPP; (c) EDS analysis of M-CA/JEPP. (f) EDS mapping of M-CA/JEPP

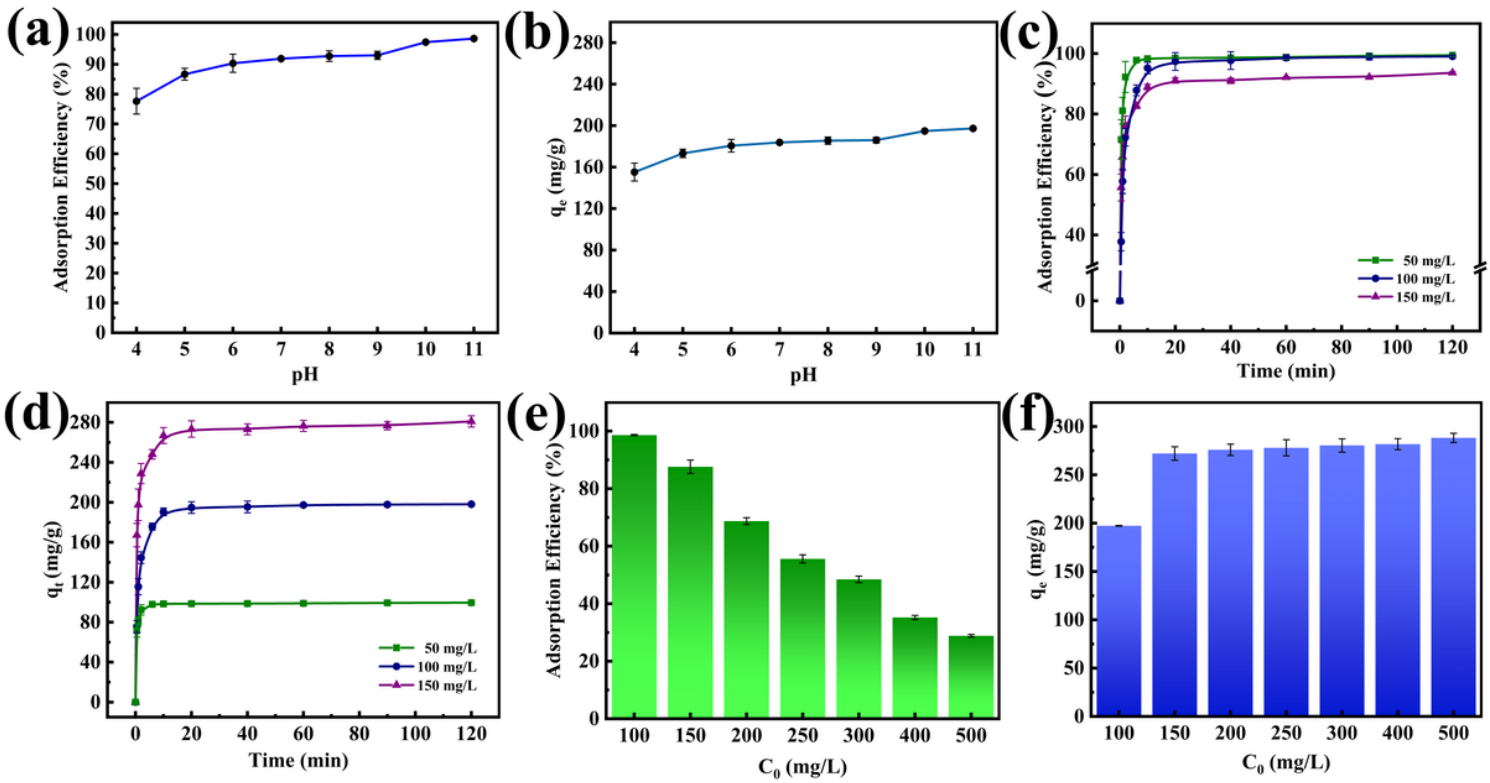


Figure 3

The adsorption efficiency (a) and the equilibrium adsorption capacity (b) of MB at different initial pH (4-11), initial dye concentration of 100 mg/L, 303 K and 10 mg of adsorbents. The adsorption efficiency (c) and the adsorption capacity (d) of MB in different time, initial pH=11, initial dye concentration of 50 mg/L, 100 mg/L and 150 mg/L, 303 K and 10 mg of adsorbents. The adsorption efficiency (e) and the equilibrium adsorption capacity (f) of MB towards different initial dye concentration in 60 min, initial pH=11, 303 K and 10 mg of adsorbents

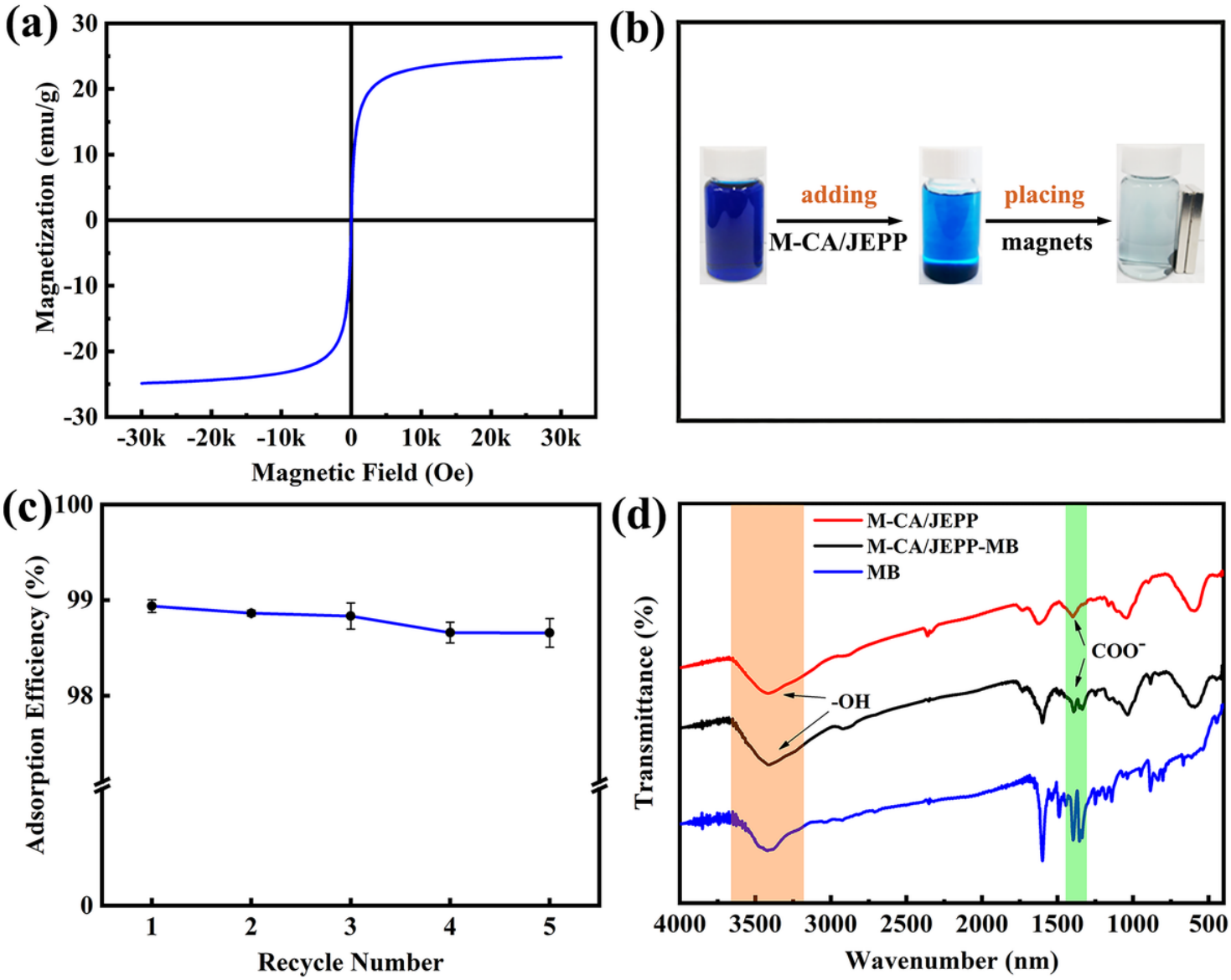


Figure 4

(a) Magnetization curve of M-CA/JEPP. (b) Digital photo of separation after adsorption by magnets, initial pH=11, initial dye concentration of 50 mg/L, 303 K and 10 mg of adsorbents. (c) Regeneration performance of M-CA/JEPP. (d) FTIR spectra of M-CA/JEPP,M-CA/JEPP-MB, and MB

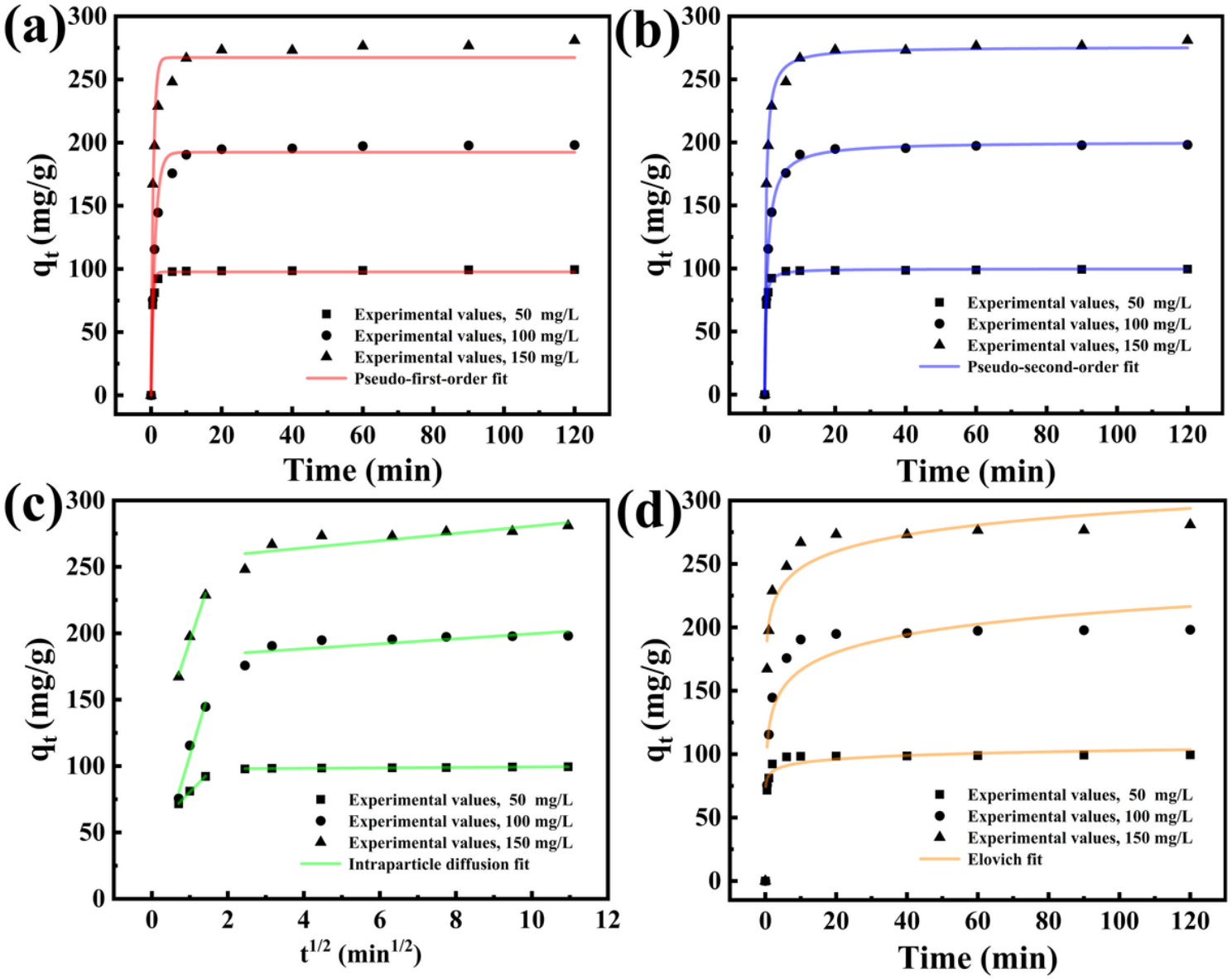


Figure 5

Adsorption kinetics data of M-CA/JEPP for MB fitted with (a) Pseudo-first-order, (b) Pseudo-second-order, (c) Intraparticle diffusion, (d) Elovich

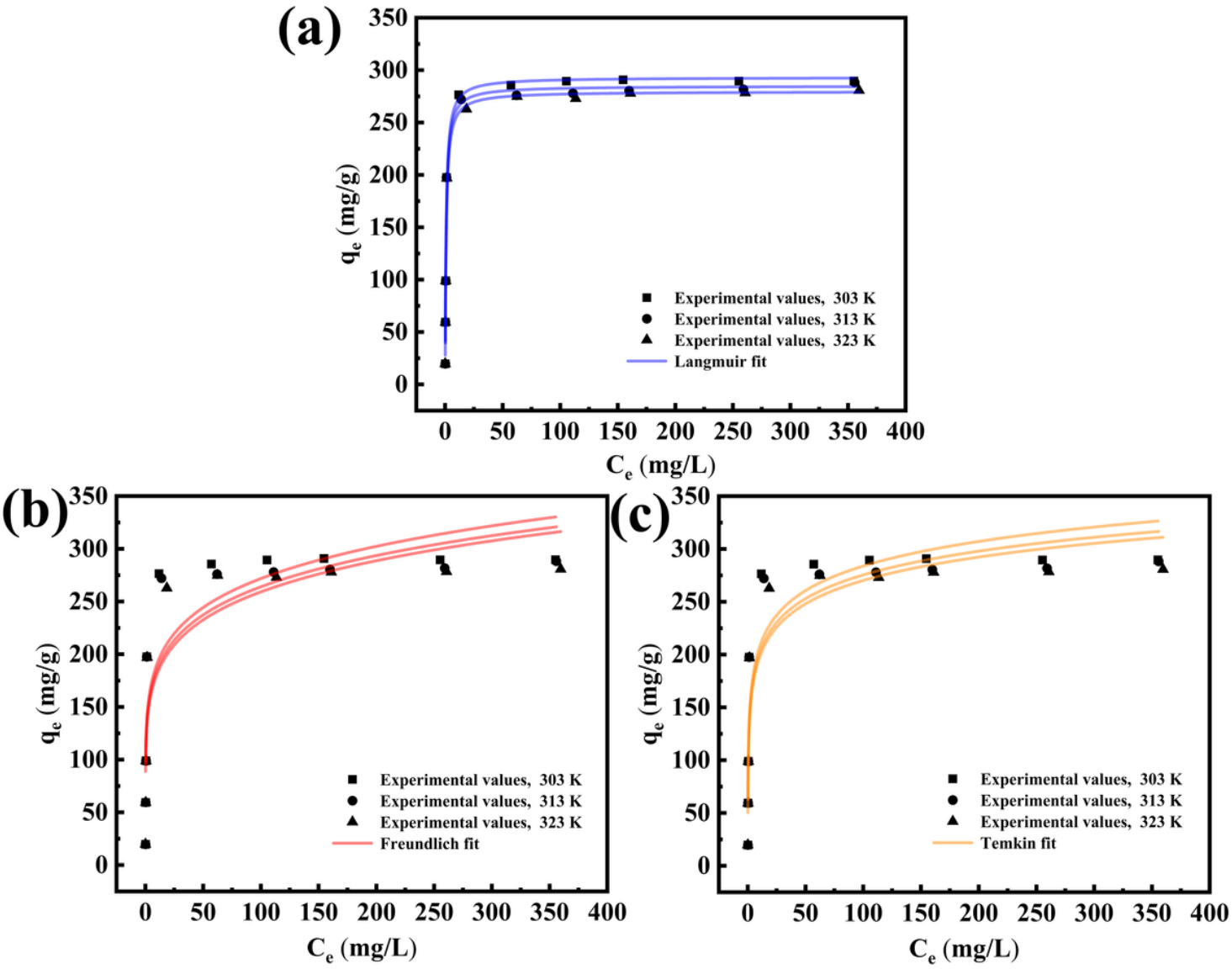


Figure 6

Adsorption isotherm data of M-CA/JEPP for MB fitted with (a) Langmuir, (b) Freundlich, (c) Temkin

Supplementary Files

This is a list of supplementary files associated with this preprint. Click to download.

- SupportingInformation.pdf
- floatimage1.png
- floatimage6.png